Evaluation of the transient response and implementation of a heading-angle controller for an autonomous ground vehicle

Shubhashisa Sahoo[1], Shankar C Subramanian[2] and Suresh Srivastava[3]

Abstract

In this paper, a dynamic mathematical model of an autonomous ground vehicle was used to analyse its transient response and to design a heading-angle controller for the vehicle. A suitable 'control-oriented model' that could accurately characterize the phenomenon of interest was used to design the controller. The efficacy of this model was evaluated by corroborating its results with experimental data. This model included the cornering stiffness of the tyres as an unknown parameter, and two approaches were attempted to estimate its value. The dynamics of the actuator were included in the analysis since the response time to steer the front wheel is of the same order as that of the heading-angle dynamics of the vehicle. The performance of two controllers (namely a classical transfer-function-based controller and an optimal linear quadratic regulator) were evaluated using the IPG: CarMaker® simulation platform over a range of speeds. The transfer-function-based controller was also implemented on the experimental test vehicle at low speeds (high-speed experimental implementation was not possible because of safety concerns). It was found that control gain scheduling helped to track the desired heading angles of the vehicle at various speeds. Subsequently, a lane-change manoeuvre using the test vehicle was performed to evaluate the controller further. It was found that the transfer-function-based heading-angle controller could provide a comparable performance with that of the linear quadratic regulator, while keeping the sensing requirements to a minimum; thus, it was suitable for real-time implementation in an autonomous ground vehicle.

Introduction

With the advent of increasing attention to surveillance, search and rescue operations in hazardous environments, militant insurgency, mine detection, mine clearance, etc., the navigation of autonomous ground vehicles (AGVs) has attracted much attention in recent years.[1–3]

Significant research and development programmes have been established during the past few years to develop fully autonomous ground vehicles, but the technologies are not ready for immediate use. The first grand challenge of the Defense Advanced Research Projects Agency (DARPA) took place in March 2004 to spur innovation in autonomous navigation.

The challenge was to develop an AGV that would complete a 230 km off-road stretch in less than 10 h. The racecourse was described with 2586 waypoints as longitude–latitude pairs coupled with a corridor width and allowable speed limits. No vehicle was able to complete the 2004 DARPA grand challenge.[4] The vehicle named 'Sandstorm', which used a pure pursuit algorithm based on a geometric method for path tracking, went the farthest. In the 2005 DARPA grand challenge, only five vehicles were able to complete the racecourse which was similar to that of the 2004 competition. The vehicle 'Stanley' that won the DARPA grand challenge

[1]Centre for Artificial Intelligence and Robotics, Defence Research & Development Organization, Bengaluru, India
[2]Department of Engineering Design, Indian Institute of Technology Madras, Chennai, India
[3]Office of the Director General – Aeronautics, Defence Research & Development Organization, Bengaluru, India

Corresponding author:
Shankar C Subramanian, Department of Engineering Design, Indian Institute of Technology Madras, Chennai 600036, India.
Email: shankarram@iitm.ac.in

in 2005 used a steering control law based on a kinematic bicycle model. 'Boss', the autonomous vehicle that won the DARPA Urban Challenge in 2007, used a predictive control strategy to complete the 96 km urban racecourse in less than 6 h. The steering controller was developed on the basis of a kinematic model of the vehicle, including a time delay and rate limits on the steering wheel.[5]

The dynamic response of the vehicle plays a significant role in designing the lateral controller for an AGV since it depends on the vehicle parameters, the road information and also the steering actuator dynamics. To analyse the behaviour of the vehicle in various driving conditions, different types of vehicle model are available in commercial vehicle simulation software packages such as ADAMS/Car, CarSim[TM] and IPG/CarMaker[®]. However, it is usually difficult to obtain the values of all the parameters used in the simulations from vehicle manufacturers. Furthermore, most of these software packages use the 'magic formula'[6] or other semiempirical tyre models. In reality, an extensive experimental facility is required to determine the coefficient values used in these tyre models. Although a simulation model is an abstraction of the actual system, the controllers are designed relative to these models and then deployed on the real system. Therefore, the accuracy of the performance of the controller depends on, among other factors, the accuracy of the parameter values used in that model. Hence, a vital step in controller design is the development of a suitable 'control-oriented model' which can accurately characterize the phenomenon of interest while ensuring that the developed controller is tractable for real-time implementation.

Continuum motion generation algorithms have not taken into account the effects of the slip angle of the vehicle, the ground–wheel interaction, the steering actuator dynamics and the control gain limits at the level of primitive motions. Dubins[7] showed that a sequence of three path segments, which are either an arc of a circle or a straight-line segment, is the shortest path for a forward-moving vehicle at a constant speed. Later, Reeds and Shepp[8] generalized this result to forward and backward motions and defined a set of 48 paths which contains the optimal path. Schroder et al.[9] used the Dubins method with different start circles and goal circles for path planning of cognitive vehicles using risk maps. These studies have been restricted to line and arc primitives based on the quest for the shortest path. In these methods, the steering angle was also assumed to change instantaneously during transition between consecutive path curvatures. Therefore, if the actual motion is admissible or even possible at all, a greater control effort is required at the implementation level. By using a dynamic model of the vehicle, a significant source of error can be eliminated at the planning level rather than reactively at the implementation level.

Coombs et al.[10] commanded an AGV to follow a set of simple straight-line segmented obstacle-free paths. They found that their approach worked well at low speeds but was unstable at higher speeds. Latencies associated with sensor update rates and discretization of the path contributed to the problem. For a longitudinal speed of the vehicle greater than 7.5 m/s, they used sequences of segmented clothoidal paths by simulating the vehicle trajectories resulting from a sequence of steering rate commands and a range of vehicle speeds. However, they have not discussed much about the implementation and control aspects. In related work, Suppachai et al.[11] demonstrated control of the heading angle of a vehicle at speeds of 1 m/s and 3 m/s. Since the steering actuator dynamics were not considered while designing the controllers, the reference path waypoints were also found to change more quickly than the rate at which the steering wheel can turn. Lee et al.[12] applied system identification techniques to obtain a system model after receiving the data from the Differential Global Positioning System and an electric compass. While simulating the model, a first-order linear transfer function was used as the dynamic model for the steering actuator. The overshoots in the yaw angles with both a proportional–integral–derivative controller and an H_∞ controller were more than 10% for a step response. Therefore, it is important to design a controller that considers the steering actuator dynamics accurately together with the appropriately estimated model parameters.

Many estimation methods available in the literature had assumed that the steering angle, the side-slip angle and the yaw rate are measured or observed. Many of these estimation methods were simulated in commercially available software packages.[13] In the case of real applications and practical implementation, a specific and expensive device is required to measure the lateral velocity of the vehicle's side-slip angle. A comparatively expensive wheel force measurement is required to measure the lateral force or the lateral acceleration of the vehicle. In addition to that, a large-area test facility is also required to test the validity of these methods at higher speeds.

Wesemeier and Isermann[14] described a method of estimating the cornering stiffness of the tyres from the measurement of the vehicle speed, the lateral acceleration, the yaw rate and the vehicle's side-slip angle. The advantage of the method is that the cornering stiffness together with the centre of gravity (CG) of the vehicle can be measured simultaneously without any knowledge of the moment of inertia of the vehicle. However, a special optical sensor is required to measure the side-slip angle of the vehicle.

Sierra et al.[15] proposed several methods to estimate the cornering stiffness on the basis of the simulation data from the bicycle model and the CarSim software. Each method has its own specific advantages and limitations related to practical implementations. Among those methods, except for the beta-less method[16] (i.e. a method which does not depend on the side-slip angle), all other methods require the lateral velocity of the vehicle (or, equivalently, the side-slip angle), which is

difficult to measure reliably in real scenarios. In addition, these methods are under-determinate in nature, and persistent excitation is required to obtain accurate results.

Kutluay and Winner[17] presented a survey on the validation of simulation models for vehicle dynamics. They reported that, although simulation environments and mathematical theories on vehicle dynamics are well established, the methodical link between the experimental test data and the validity analysis of the simulation model is still lacking. They claimed that neither a standard in experimentation and data-handling processes in the modelling of vehicle dynamics nor a standard reasoning process in the modelling application of vehicle dynamics exists in validation analysis. The validation criteria are dependent on the application, and the data-handling methods are dependent on the chosen manoeuvres.

Kazemi and Shirazi[18] presented the simulation of a four-wheel steering vehicle with sliding-mode control. The desired yaw rate was used as the reference input for designing the control system. It was observed from simulations that the improvement in the handling of sliding-mode control is more effective at higher speeds (40–60 m/s). However, there was a steady-state error in J-turn and fishhook manoeuvres with both a two-wheel steering vehicle and a four-wheel steering vehicle with sliding-mode control.

Ba et al.[19] developed a controller based on the recursive optimized version of the predictor-based subspace identification method in which the vehicle model can be identified from input–output data. In comparison with traditional predictive controllers, the proposed methods are effective for vehicle control in the linear domain. However, because of the many matrix operations and recursive identification at each step, there was a time delay for vehicle control, and the action of the controllers was not sufficiently fast to track the rapidly changing desired values.

Du et al.[20] designed a velocity-dependent controller where the range of forward velocities was varied from 10 m/s to 40 m/s. Numerical simulations were carried out using the planar two-degree-of-freedom (2DOF) vehicle dynamics model with the non-linear Dugoff tyre model to validate the effectiveness of the proposed controller. As the side-slip angle was controlled to within 2°, the corrected linear tyre model could cover most road conditions, and the designed controller made the lateral dynamics of the vehicle insensitive to the variation in road conditions. However, vehicle rollover was not considered in the simulations of the J-turn manoeuvre, which was produced from the ramp steering input (the maximum is 6°) at a much higher speed.

Mirzaei[21] presented a model for vehicle handling based on the linear 2DOF model. The tyre and road conditions were tracked by the direct yaw moment control system. When the side-slip was controlled in the simulations, the yaw rate response was autonomously restricted, and consequently the whole vehicle motion became stable. However, because of the impracticality of the direct measurement of the side-slip angle, online estimation of this state variable must be made.

Attia et al.[22] proposed non-linear model predictive control for simultaneous longitudinal control and lateral control. The whole control strategy was tested using simulations showing the effectiveness of the approach.

Janbakhsh et al.[23] proposed a new method of non-linear adaptive dynamic surface sliding control for simultaneous vehicle-handling and path-tracking improvement through simulations of a steer-by-wire system. The constant sliding gain in the traditional sliding-mode scheme was replaced with a time-variant value estimated through an adaptation law.

Yakub and Mori[24] showed that model predictive control was more useful than linear quadratic control for multi-variable systems and for systems with constraints. However, when the vehicle behaviour was simulated on a low-road-adhesion surface, there was a trade-off for the controllers to achieve the target for two tracking outputs with one control signal.

From the literature survey, it was found that most studies related to heading-angle control for an AGV were simulations without practical implementation. A challenge is the measurement of the side-slip angle for real-time implementation. In order to address this important issue, this study compared the performances of two controllers; the first controller is a classical transfer-function-based proportional controller and the second is a controller based on the linear quadratic regulator (LQR). The classical transfer-function-based controller does not require the measurement of the side-slip angle for its implementation, while the LQR controller does requires the measurement of the side-slip angle. Given the difficulties in measuring the side-slip angle of the test vehicle, the LQR framework was evaluated using the IPG: CarMaker simulation platform. However, the proportional controller was implemented on this simulation platform as well as on the experimental test vehicle. It was found that the proportional controller can provide a comparable performance with respect to the LQR controller, which renders it suitable for real-time implementation. This is an important finding from this study since it prescribes the use of a simple proportional controller for real-time heading-angle control of an AGV, which does not require the measurement of the side-slip angle while providing a good performance.

Overall, this paper presents the development and real-time implementation of a heading-angle controller for an AGV using a control-oriented model that can accurately characterize the phenomenon. A linear 2DOF vehicle model, together with a suitable steering actuator model, was considered for this purpose. Two approaches were used to estimate the cornering stiffness of the tyres. The performance of the model with estimated parameters was evaluated using experimental data. The two controllers were designed and the

controller gains were scheduled with respect to the longitudinal speed of the vehicle to improve the tracking performance. Finally, the proportional controller was implemented on an AGV equipped with the Global Positioning System (GPS) and an inertial measurement unit (IMU) to evaluate its real-time performance.

Test vehicle

In this study, a commercially available four-wheeled battery-operated vehicle was modified for use as the test vehicle. The front and top parts of the vehicle body were modified to accommodate the necessary electronics and sensors. Electric power was supplied from a 48 V d.c. battery bank that can drive the vehicle with a maximum speed of 20 km/h. The test platform after modification and mounting of the equipment is shown in Figure 1.

The steering system is a self-adjusting rack-and-pinion steering system. To control the heading, the conventional steering system was converted to a drive-by-wire system by installing a d.c. motor (Maxon RE-40) with a 156:1 reduction gear ratio at the steering shaft. The rotation of the steering shaft can be measured using the encoder attached to the steering actuator. The steering actuator was connected to the steering shaft with the help of spur gears with a gear reduction ratio of 1.47. The standard rack-and-pinion steering system of the vehicle has a gear ratio of 15.5. The vehicle controller interprets the position of the accelerator pedal mechanism to control the wheel motor speed. This was modified to accept an input voltage generated from a higher-level controller rather than from the accelerator pedal itself.

The primary means of localization is by the use of the GPS. NovAtel's GPS-702-GGL antenna allows improved positioning accuracy provided by L-band technology. It was mounted on the roof of the vehicle. To cater for probable eventualities such as GPS inaccuracy, outage or denial, the system also has an accurate inertial navigation system (INS) onboard, which augments and is augmented by the GPS. The INS consists of a gyro-stabilized compass and an iMAR-FSAS. The iMAR-FSAS is a tactical-grade IMU from iMAR GmbH. The IMU measurements were sent to the NovAtel synchronized position attitude navigation (SPAN)-enabled ProPak-V3[TM] GPS receiver to generate reliable position, velocity and attitude measurements[25] up to 200 Hz.

Simulation model of the vehicle dynamics

This section describes the mathematical modelling process to obtain the heading-angle transfer function and the model of the steering subsystem under the following assumptions. Pitching and rolling motions were ignored. At low speeds, aerodynamic drag was neglected. Further, in most of the manoeuvres such as a lane change, step steering and a constant-radius turn, the longitudinal speed of the vehicle remains almost constant. In addition to the aforementioned assumptions, when the weight is equally distributed on either side of the vehicle, the well-known dynamic bicycle model can be used. This model combines the effects of the two wheels on the same axle and treats them as a single wheel. A schematic diagram of the bicycle model considered in this study is shown in Figure 2.

The lateral position of the vehicle is measured along the lateral axis of the vehicle, and the yaw angle of the vehicle is measured with respect to the global X axis. The 2DOFs are represented by the vehicle's lateral position y and the vehicle's heading angle θ. The lateral force at the tyre–road interface depends on the slip

Figure 1. Test vehicle.
UPS: uninterruptible power supply; IMU: inertial measurement unit; GPS: Global Positioning System; 3D: three-dimensional; 2D: two-dimensional; SBW: steer-by-wire.
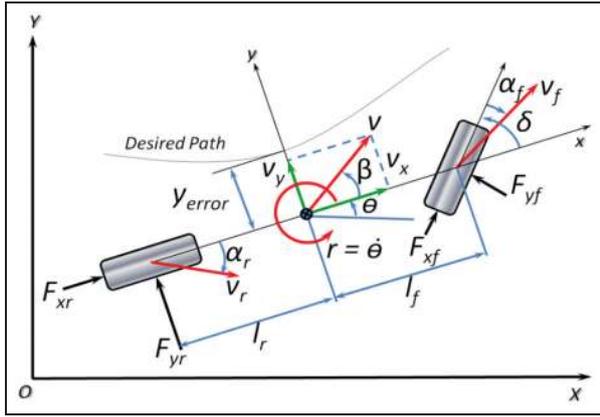
$$\begin{bmatrix} \dot{\beta} \\ \dot{r} \end{bmatrix} = \begin{bmatrix} -\frac{C_f + C_r}{mv_x} & -1 - \frac{C_f l_f - C_r l_r}{mv_x^2} \\ -\frac{C_f l_f - C_r l_r}{I_z} & -\frac{C_f l_f^2 + C_r l_r^2}{I_z v_x} \end{bmatrix} \begin{bmatrix} \beta \\ r \end{bmatrix} + \begin{bmatrix} \frac{C_f}{mv_x} \\ \frac{C_f l_f}{I_z} \end{bmatrix} \delta$$

(5)

Figure 2. Dynamic bicycle model.

angle. It was assumed that only the front wheel is steerable. Considering the steering angle δ to be small, the lateral motion and the yaw motion of the vehicle are governed by

$$m(\dot{v}_y + v_x r) = F_{yf} + F_{yr} \tag{1}$$

and

$$I_z \dot{r} = l_f F_{yf} - l_r F_{yr} \tag{2}$$

where m is the mass of the vehicle, v_x and v_y are the longitudinal velocity and the lateral velocity respectively of the vehicle, I_z is the yaw moment of inertia of the vehicle, r is the yaw rate of the vehicle, F_{yf} and F_{yr} are the lateral force on the front tyre and the lateral force on the rear tyre respectively, l_f and l_r are the distance of the front tyre from the vehicle's CG and the distance of the rear tyre from the vehicle's CG. Experimental results show that the lateral tyre force is proportional to the slip angle for small slip angles.[6] The slip angle is defined as the angle between the orientation of the tyre and the direction of the velocity vector at that tyre. For small slip angles α_f of the front wheel and small slip angles α_r of the rear wheel, the lateral force acting on the front wheel and the lateral force acting on the rear wheel can be written as

$$F_{yf} = C_f \alpha_f, \quad F_{yr} = C_r \alpha_r \tag{3}$$

where C_f and C_r are the cornering stiffness of the front tyre and the cornering stiffness of the rear tyre respectively. On the assumption that the side-slip angle of the vehicle is given by $\beta \approx v_y/v_x$, the slip angle of the front wheel and the slip angle of the rear wheel are

$$\alpha_f = \delta - \left(\beta + \frac{l_f r}{v_x}\right), \quad \alpha_r = -\left(\beta - \frac{l_r r}{v_x}\right) \tag{4}$$

Using equations (1) to (4), the governing equation becomes

Heading-angle transfer function

The transfer function $G_\delta^r(s)$, which relates the response of the yaw rate to the steering angle, was obtained as

$$G_\delta^r(s) = \frac{a_1 s + a_2}{s^2 + 2\xi\omega_n s + \omega_n^2} \tag{6}$$

where

$$a_1 = \frac{C_f l_f}{I_z}$$

$$a_2 = \frac{C_f C_r l}{mI_z v_x}$$

$$2\xi\omega_n = \frac{m\left(C_f l_f^2 + C_r l_r^2\right) + I_z(C_f + C_r)}{mI_z v_x}$$

and

$$\omega_n^2 = \frac{C_f C_r l^2}{mI_z v_x^2} - \frac{C_f l_f - C_r l_r}{I_z}$$

The transfer function $G_\delta^\theta(s)$, which relates the response of the heading angle to the steering angle, was obtained as

$$G_\delta^\theta(s) = \frac{a_1 s + a_2}{s(s^2 + 2\xi\omega_n s + \omega_n^2)} \tag{7}$$

The understeering coefficient K_{us} can be written as

$$K_{us} = \frac{W_r}{C_f} - \frac{W_f}{C_r} \tag{8}$$

where W_f is the normal load on the front tyres and W_r is the normal load on the rear tyres. If $K_{us} > 0$, the vehicle is in understeering mode; if $K_{us} = 0$, the vehicle is in neutral-steering mode; if $K_{us} < 0$, the vehicle is in oversteering mode.

The transfer function $G_\delta^\beta(s)$, which relates the response of the side-slip angle to the steering angle, was obtained as

$$G_\delta^\beta(s) = \frac{b_1 s + b_2}{s^2 + 2\xi\omega_n s + \omega_n^2} \tag{9}$$

where

$$b_1 = \frac{C_f}{mv_x}$$

and

$$b_2 = \frac{C_f C_r l_r l - C_f l_f m v_x^2}{mI_z v_x^2}$$

Longitudinal model for vehicle start-up

A longitudinal model of the vehicle was included when the vehicle starts from rest. There was no steering input until the vehicle achieved a constant velocity. After the vehicle achieved a constant velocity, the bicycle model of the vehicle was used. When the vehicle starts from rest to achieve a constant speed, a first-order process model with a time delay was used to represent the evolution of the longitudinal speed. The transfer function $G_{des}^{v}(s)$, which relates the response of the actual longitudinal velocity to the desired velocity of the vehicle, was obtained as

$$G_{des}^{v}(s) = e^{-T_d s} \frac{K}{T_p s + 1} \tag{10}$$

where K is the velocity gain, T_d is the time delay and T_p is the time constant. Using the first-order Padé approximation to obtain the steady-state longitudinal velocity, equation (10) can be written as

$$G_{des}^{v}(s) \approx \frac{1 - s(T_d/2)}{1 + s(T_d/2)} \frac{K}{T_p s + 1} \tag{11}$$

From experiments conducted at different longitudinal speeds ranging from 1.7 m/s to 3.8 m/s, it was found that the values are as follows: the velocity gain $K = 1$, the time delay $T_d = 0.66$ s and the time constant $T_p = 2.2$ s. Let (X, Y) be the coordinates of the vehicle's CG with respect to the axis fixed on the ground. Then

$$\dot{X} = v \cos(\beta + \theta) \tag{12}$$

and

$$\dot{Y} = v \sin(\beta + \theta) \tag{13}$$

By integrating equations (12) and (13), the position of the vehicle's CG can be estimated.

Determination of the vehicle parameters

From equation (6), it can be observed that the transfer function coefficients depend on the vehicle parameters. The dynamic mass transfer between the front wheel and the rear wheel was neglected for low-acceleration operations. The total mass of the vehicle, the CG location and the moment of inertia were estimated by measuring the vehicle's split mass, utilizing four measuring scales under each wheel. The total mass m of the vehicle is the sum of the measurements of mass under each wheel. Using these values and a measurement of the wheelbase l, the location of the CG is described by the distance l_f from the front axle and the distance l_r from the rear axle along the centre-line. The moment of inertia of the vehicle was calculated by treating the vehicle as two point masses joined by a massless rod. The specification data for the test vehicle are listed in Table 1.

However, accurate determination of the cornering stiffness of the tyres requires extensive experiments. In this study, to predict the vehicle behaviour in a real

Table 1. Parameters of the test vehicle.

Parameter	Value	Units
Mass m_{fl} at the front left wheel	158	kg
Mass m_{fr} at the front right wheel	137	kg
Mass m_{rl} at the rear left wheel	360	kg
Mass m_{rr} at the rear right wheel	269	kg
Mass m of the vehicle	924	kg
Wheelbase l	1.93	m
Location l_f of the centre of gravity from the front axle	1.31	m
Location l_r of the centre of gravity from rear the axle	0.62	m
Moment I_z of inertia	748	kg m^2

Table 2. Parameters of the tyre.

Parameter	Value	Units
Aspect ratio a of the tyre	0.5	—
Thickness b of the tyre belt	0.015	m
Compression modulus E of the belt	27×10^6	N/m^2
Radius r_w of the wheel	0.254	m
Unitized percentage s of the sidewall vertical deflection when loaded	15	%
Width w of the belt	0.205	m

environment and to evaluate the performance of the designed controller, the cornering stiffness of the tyres was estimated as described below.

Estimating the cornering stiffness of the tyres from basic tyre information. It is necessary for the tyre manufacturer to print certain information such as the wheel radius, the tyre width, the aspect ratio (which is the ratio of the tyre section height to the tyre width expressed as a percentage), the load index, the speed rate, the type of tyre construction and the maximum allowed inflation pressure, on the tyre sidewall. From this basic tyre information, the cornering stiffness can be estimated by using a mathematical tyre model.[26] The final expressions that were used to estimate the cornering stiffness C_α of the tyres are

$$C_\alpha = \frac{8Ebw^3}{L[2\pi(r_w + wa) - L]} \tag{14}$$

and

$$L = 2(r_w + wa) \sin\left[\cos^{-1}\left(1 - \frac{swa}{r_w + wa}\right)\right] \tag{15}$$

where E is the compression modulus of the belt, b is the thickness of the tyre belt, r_w is the radius of the wheels, w is the width of the belt, a is the tyre aspect ratio (the tyre section height divide by the tyre section width), L is the contact patch length and s is the unitized percentage of the sidewall vertical deflection when loaded. The parameters of the tyres that were used to calculate the cornering stiffness are given in Table 2.

Substituting the values of the tyre parameters from Table 2 into equations (14) and (15), the cornering stiffness of the tyre was obtained as 132,600 N/rad. Since all the four tyres used in the test platform have the same specifications, the cornering stiffness of the front tyres and the cornering stiffness of the rear tyres have the same value.

Estimating the cornering stiffness of the tyres assuming that the vehicle is a neutral-steering vehicle. This proposed estimation method uses the transfer function relating the steering angle δ to the yaw rate r, as described in equation (6). Even if this method might also work for the transfer function relating the steering angle δ to the side-slip angle β, measuring the yaw rate is more feasible in practice than measuring the lateral velocity. When the cornering stiffness of the tyres is normalized by the vertical load,[27] the same vehicle would be considered as a neutral-steering vehicle according to

$$C_f l_f - C_r l_r = 0 \tag{16}$$

Then, equation (5) can be rewritten as

$$\begin{bmatrix} \dot{\beta} \\ \dot{r} \end{bmatrix} = \begin{bmatrix} -\frac{C_f + C_r}{mv_x} & -1 \\ 0 & -\frac{C_f l_f^2 + C_r l_r^2}{I_z v_x} \end{bmatrix} \begin{bmatrix} \beta \\ r \end{bmatrix} + \begin{bmatrix} \frac{C_f}{mv_x} \\ \frac{C_f l_f}{I_z} \end{bmatrix} \delta \tag{17}$$

The transfer function $G_\delta^r(s)$, which relates the response of the yaw rate r to the steering angle δ, was obtained as

$$G_\delta^r(s) = \frac{C_f l_f / I_z}{s + \left(C_f l_f^2 + C_r l_r^2 \right) / I_z v_x} \tag{18}$$

As $C_f l_f - C_r l_r = 0$, it was found that $m_f l_f = m_r l_r$. In addition to this condition, the vehicle's moment of inertia was approximated by treating the vehicle as two point masses joined by a massless rod. Therefore,

$$\begin{aligned} I_z &= m_f l_f^2 + m_r l_r^2 \\ &= m_f l_f^2 + m_f l_f l_r \\ &= m_f l_f l \end{aligned} \tag{19}$$

Hence, the transfer function $G_\delta^r(s)$ can be written as

$$\begin{aligned} G_\delta^r(s) &= \frac{C_f l_f / m_f l_f l}{s + C_f / m_f v_x} \\ &= \frac{r_{ss}}{t_r s + 1} \end{aligned} \tag{20}$$

where the steady-state yaw rate r_{ss} is

$$r_{ss} = \frac{v_x}{l} \tag{21}$$

and

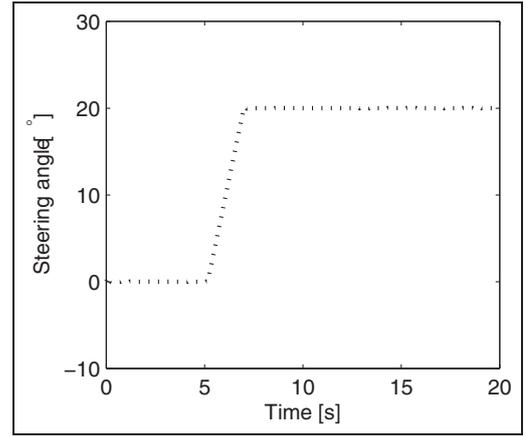$$t_r = \frac{m_f v_x}{C_f} \tag{22}$$

Figure 3. Experimental steering-angle input at the front wheel for the J-turn manoeuvre at 3.1 m/s.

The proposed method uses the available vehicle parameters (the mass m_f at the front axle and the wheelbase l of the vehicle) and the measurements (the steering angle δ, the yaw rate r and the longitudinal velocity v_x of the vehicle) to obtain the transfer function $G_\delta^r(s)$. The advantage of this method is that it does depend on the derivative of the yaw rate. Using the data from a J-turn manoeuvre, where the steering angle is the input and the yaw rate is the output, the parameters of the transfer function shown in equation (18) were obtained. The autoregressive–moving-average (ARMA) model that best describes the transfer function $G_\delta^r(s)$ was estimated by specifying the steady-state yaw rate r_{ss} which is known from measurement of the longitudinal velocity. After identifying the transfer function $G_\delta^r(s)$ from the J-turn manoeuvre, the cornering stiffness C_f of the front tyre can be calculated from the value of the coefficient t_r. Then, the cornering stiffness C_r of the rear tyre can then be calculated using equation (16).

A J-turn manoeuvre was performed on the test vehicle to estimate the cornering stiffness of the tyres. Initially, the vehicle was allowed to move for 5 s in a straight line to achieve a constant speed of 3.1 m/s. Then a steering input of 20° was provided to the front wheel of the vehicle. Figure 3 shows the steering-angle input to the front wheel of the vehicle that was measured by the encoder attached to the steering actuator. The yaw rate and the longitunial velocity of the vehicle were measured by using the INS and the GPS. The measured yaw rate of the vehicle is shown in Figure 4.

Using the system identification toolbox in MATLAB, with the measured data plotted in Figures 3 and 4, the transfer function $G_\delta^r(s)$, which best describes the continuous-time first-order ARMA model, was obtained as

$$G_\delta^r(s) = \frac{1.63}{0.02s + 1} \tag{23}$$

The estimated yaw rate was found to have an 89.9% fit to the experimental data. The difference between the

estimated yaw rate and the measured yaw rate (filtered) is shown in Figure 5. While estimating the yaw rate, the data for the initial 4 s were not considered since the vehicle had not reached a constant longitudinal velocity. After identifying the transfer function $G_\delta^r(s)$, the cornering stiffness of the tyres can be calculated from t_r. The values of the estimated cornering stiffness are presented in Table 3.

Modelling the steering actuator

The time taken for steering the front wheel by 10° is around 1 s and, since this is of the same order as the response time of the vehicle-heading dynamics, the model of the steering actuator was included in this study. In order to incorporate the actuator dynamics in

Figure 4. Experimental yaw rate for the J-turn manoeuvre measured at 3.1 m/s.

Figure 5. Yaw rate error for the J-turn manoeuvre.

the control design process, an appropriate model was derived from first principles.[28] The specification data for the steering actuator used are listed in Table 4.

The transfer function $G_V^\phi(s)$, which relates the response of the angle $\phi(s)$ of rotation of the steering motor shaft to the input voltage $V(s)$, was derived as

$$G_V^\phi(s) = \frac{1}{s}\frac{302}{0.044\,s + 9.164} \qquad (24)$$

Corroboration using the J-turn manoeuvre

Before designing the heading-angle controller for the AGV, an open-loop J-turn manoeuvre was conducted on the test vehicle to corroborate the model developed. Substituting the vehicle parameters from Table 1 and the cornering stiffness of the tyres from Table 3, the heading angle and the side-slip angle of the AGV were obtained from equation (7) and equation (9) respectively.

Let (X, Y) be the coordinates of the vehicle's CG with respect to the axis fixed on the ground. Using equations (10) to (13), the velocities in the X and Y directions were obtained and are compared with the experimental results, as shown in Figure 6. Integrating equations (12) and (13), the coordinates of the vehicle's CG were obtained. The comparison between the experimental path and the simulated path followed by the test vehicle during the J-turn manoeuvre is shown in Figure 7. As shown in Table 5, the maximum error and the r.m.s. error were less for the neutral-steering vehicle model than for the oversteering vehicle model. The maximum deviations between the simulation results and the experimental data in the X and Y directions were found to be 0.46 m and 0.31 m respectively for the neutral-steering vehicle model. The corresponding r.m.s. errors in the X and Y directions were found to be 0.23 m and 0.13 m respectively. This shows that the proposed model was able to predict the vehicle response accurately, and this was subsequently used in developing the heading-angle controller.
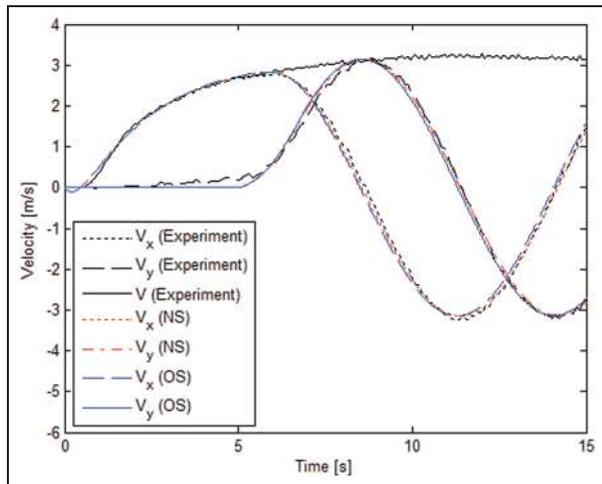
Design and implementation of the heading-angle controller

Transfer-function-based controller for the desired heading angle

From equation (7), it can be observed that the transfer function $G_\delta^\theta(s)$, which relates the response of the

Table 3. Cornering stiffnesses of the tyres.

Estimation method	Cornering stiffness	Value (N/rad)	Understeering coefficient
Neutral-steering vehicle	Front tyres, C_{fN}	46,402	$K_{us} = 0$ (neutral steering)
Neutral-steering vehicle	Rear tyres, C_{rN}	98,939	
Basic tyre information	Front tyres, C_{fO}	132,600	$K_{us} < 0$ (oversteering)
Basic tyre information	Rear tyres, C_{rO}	132,600	

Table 4. Parameters of the steering actuator.

Parameter	Value	Units
Terminal resistance R	0.317	Ω
Terminal inductance L	0.0823	mH
Torque constant K_t	30.2	mN m/A
Speed constant	317	(r/min)/V
Back e.m.f. constant K_b	0.0301	V/(rad/s)
Rotor inertia J	138	g cm^2
Speed/torque gradient	3.33	(r/min)/mN m
Nominal speed N	6930	r/min
Nominal torque T	170	mN m
Nominal voltage V	24	V

Table 5. Error values for the J-turn manoeuvre.

Parameter	Maximum error (m)	R.m.s. error (m)
X direction (neutral steering)	0.46	0.23
Y direction (neutral steering)	0.31	0.13
X direction (oversteering)	0.77	0.37
Y direction (oversteering)	0.48	0.25

Figure 6. Comparison of the experimental velocity responses and the simulated velocity responses for the J-turn manoeuvre. NS: neutral steering; OS: oversteering.
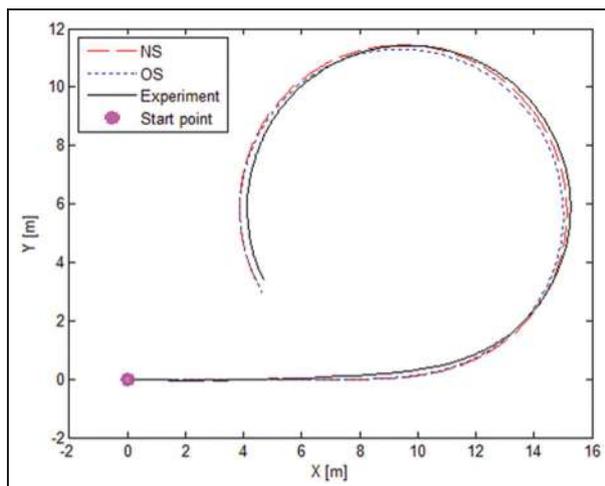
Figure 7. Comparison of the experimental path and the simulated path followed for the J-turn manoeuvre. NS: neutral steering; OS: oversteering.

heading angle to the steering angle, has a pole at the origin. To track the desired heading angle, a closed-loop negative feedback system was considered, as shown in Figure 8. This heading-angle controller will compute the required steering angle based on the error in the heading angle of the vehicle. The design criteria of the controller was to keep the steady-state error within the limit of 5% and the maximum overshoot less than 10%, with a settling-time requirement of less than 3 s.

The steering-angle input to the vehicle depends on the desired heading angle for the given speed of the vehicle. The controller designed for this system consists of two loops. The inner-loop controller, the transfer function of which is $H_V^\phi(s)$, minimizes the error between the desired angular position and the current angular position of the steering motor. The input of this loop is a function of the steering angle which is calculated on the basis of the error in the heading angle of the vehicle. The outer-loop controller, the transfer function of which is $H_\theta^\delta(s)$, decreases the error between the desired heading angle and the actual heading angle of the vehicle. The transfer function $G_\delta^\theta(s)$, which relates the response of the heading angle to the steering angle, was obtained using equation (7). The steering actuator model was derived analytically from first principles in equation (24).

The steering-angle tracking response was simulated. A saturation block was added to restrict the voltage input from –20 V to + 20 V. Data were collected for the steering wheel's response to various commanded step inputs. Again, with these data, the saturation points of the steering wheel's velocity and acceleration were determined experimentally. From the experiment, it was found that the proportional–integral steering controller with $K_{ps} = 3$ and $K_{is} = 0.2$ gave better results as the maximum error was within 5% of that of the simulated results. A wide range of experiments was conducted, and the results were compared with the simulation results.

Implementation of point-to-point navigation

For the navigation of an AGV, a point-to-point motion algorithm was considered where the error in heading angle was used to determine the steering angle. The desired speed and the heading angle of the vehicle were decided by the vehicle path planner. The state variables (X, Y, θ) can be measured from the GPS and the IMU. In this case, (X, Y) represents the position of the vehicle and θ is the heading angle of the vehicle. If the
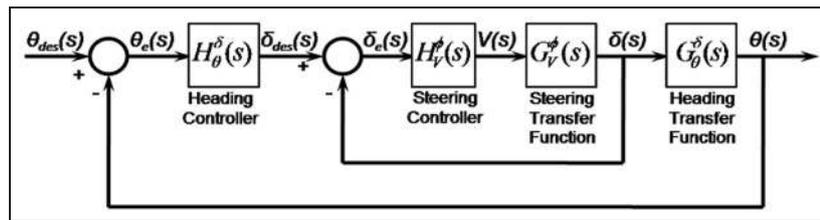
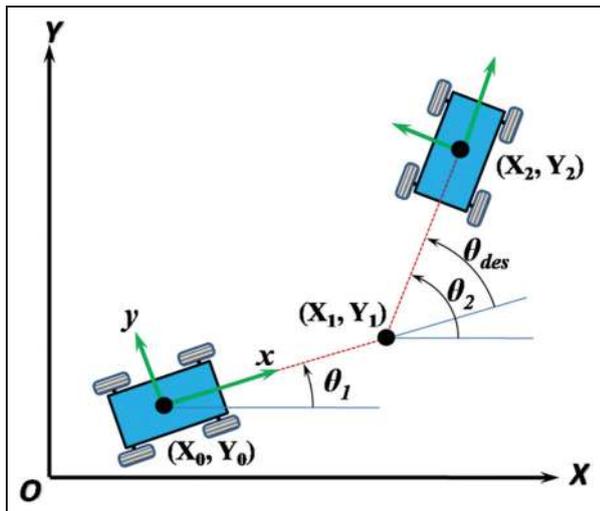**Figure 8.** Negative feedback system considering the steering actuator dynamics.
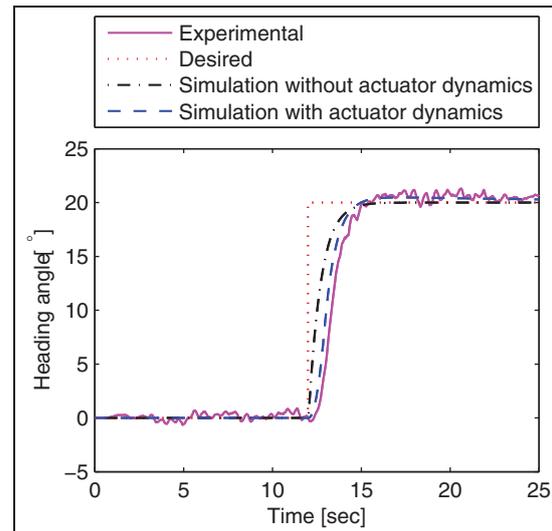

Figure 9. Point-to-point navigation.

Figure 10. Comparison of the experimental results and the simulated results of the heading-angle response for a desired heading angle of 20° with $K_p = 0.7$ when the vehicle is moving at 3.8 m/s.

waypoints on the path are known, the desired heading angle can be calculated from three consecutive GPS waypoints (X_0, Y_0), (X_1, Y_1) and (X_2, Y_2), as shown in Figure 9. The desired change θ_{des} in the heading angle of the AGV is

$$\theta_{des} = \theta_2 - \theta_1 \qquad (25)$$

For a waypoint to have been reached, the vehicle must pass it at a distance less than or equal to the radial tolerance for that waypoint. The mismatch between the desired heading angle and the actual heading angle in the real environment needs to be minimal to achieve good path tracking. In addition, this is significantly affected by the speed of the vehicle.

A proportional heading controller was designed to reduce the settling time and to keep the steady-state error within the limit of 5%. The maximum overshoot requirement of 10% of the steady-state response causes the damping ratio ζ to be less than 0.6. These conditions were translated into the desired regions of closed-loop poles and then used to tune the value of the proportional gain K_p for each vehicle velocity. For a better understanding of the system behaviour and to reduce the settling time, the tracking response of the heading angle without considering the actuator dynamics was simulated and compared with the scenarios considering actuator dynamics. The proportional gain K_p that

satisfies the performance requirements was found to be 0.7 for a vehicle speed of 3.8 m/s. The experimental and the simulation results of the heading-angle response and the steering-angle response are shown in Figure 10 and Figure 11 respectively. The position of the vehicle in the local coordinate system is shown in Figure 12.

From the experimental data in Figure 10, it was found that the settling time was 2.8 s. From Figure 11, it was observed that the maximum steering requirement was 10.2°, which is well within the steering limit of the vehicle. However, in order to achieve the desired change of 20° in the heading angle, the final heading angle of the vehicle was found to be 20.54°. Both Figure 10 and Figure 12 indicate that there was a steady-state error of 2.7% in the change in the heading angle. However, the steady-state error was found to be less than 5% and there was no overshoot.

Figure 13 shows that, in comparison with the experimental data, the maximum tracking error in the desired heading angle was 10.6° when the steering actuator dynamics were not considered in the simulations. The maximum error was reduced to 4.6° by considering the steering actuator dynamics in the simulation. The steering-angle error between the experimental and simulation results is shown in Figure 14.
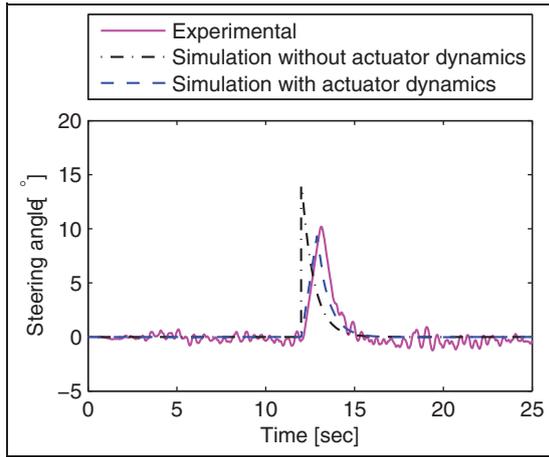
Figure 11. Comparison of the experimental results and the simulated results of the steering-angle response for a desired heading angle of 20° with $K_p = 0.7$ when the vehicle is moving at 3.8 m/s.
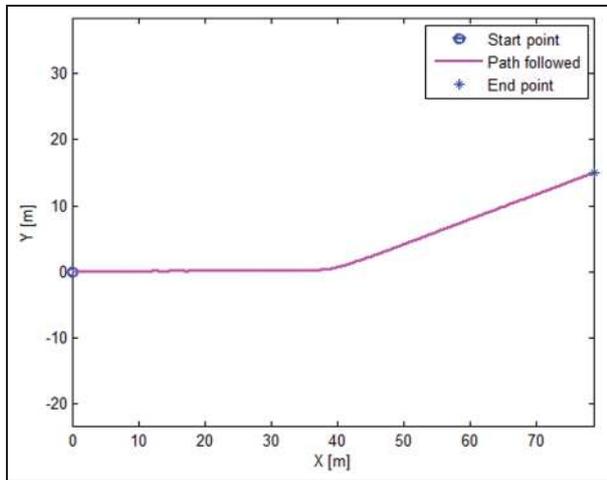

Figure 12. Position of the vehicle in the local coordinates for a desired heading angle of 20° with $K_p = 0.7$ when the vehicle is moving at 3.8 m/s.

Figure 13. Difference between the experimental heading angles and the simulated heading angles for a desired heading angle of 20° when the vehicle is moving at 3.8 m/s.

Figure 14. Difference between the experimental steering angles and the simulated steering angles for a desired heading angle of 20° when the vehicle is moving at 3.8 m/s.

Table 6. Values of K_p at various speeds of the vehicle.

Speed of the vehicle (m/s)	Value of K_p
1.7	1.0
2.4	0.9
3.1	0.8
3.8	0.7

Sensitivity analysis of the vehicle parameters

It was found that the longitudinal speed of the vehicle and the cornering stiffness of the tyres appeared in the transfer function of the heading angle of the vehicle. As the speed of the vehicle is considered to be constant for the bicycle model, the controller needs to be tuned for different speeds, and a gain-scheduling method can be considered for navigation. The sensitivity of the developed controller with respect to the longitudinal speed was studied by varying the speed values from 1.7 m/s to 3.8 m/s, keeping all the other conditions the same. To meet the design criteria, the controller gain values at different speeds of the vehicle were calculated and are presented in Table 6. The proportional gain K_p that satisfied the performance requirements was found to be 1.0 for a vehicle speed of 1.4 m/s and 0.7 for a vehicle speed of 3.8 m/s. From the simulations, it was found
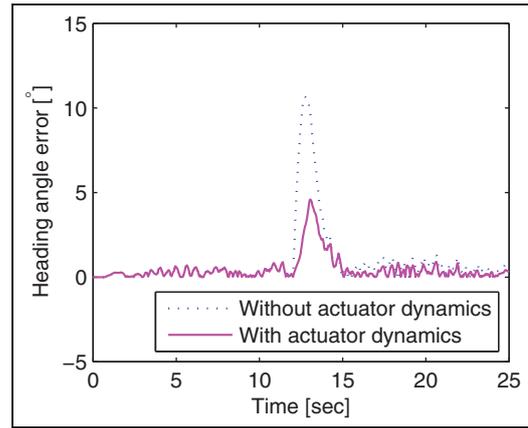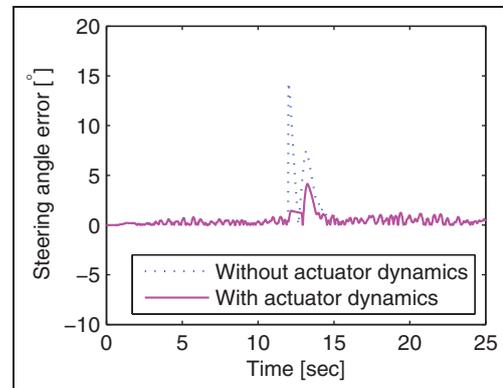
that, as the speed of the vehicle increases, the value of K_p has to be decreased in order to reduce the overshoot.

The experimental and simulated results for the heading-angle response and the steering-angle response at a speed of 1.7 m/s are shown in Figure 15 and Figure 16 respectively. To achieve the desired heading angle of 20°, it was found from Figure 15 that the settling time increased to 3.2 s as the speed of the vehicle decreased to 1.7 m/s. From Figure 16, it can be observed that the maximum steering-angle requirement increased to 14.5°. From the simulations, it can be found that, as the vehicle speed increases, the gain decreases and the maximum steering-angle requirement decreases.
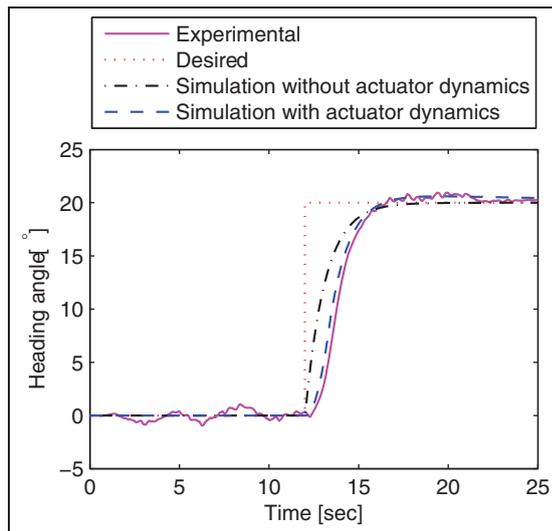
Figure 15. Comparison of the experimental results and the simulated results of the heading-angle response for a desired heading angle of 20° with $K_p = 1.0$ when the vehicle is moving at 1.7 m/s.
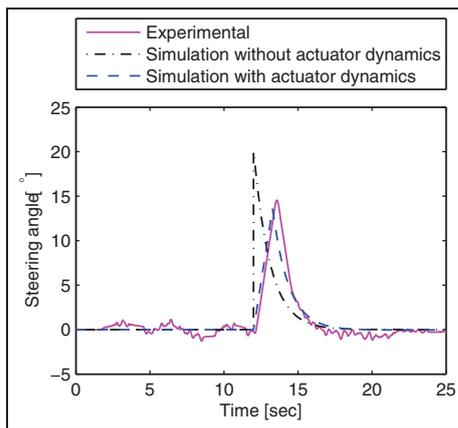

Figure 16. Comparison of the experimental results and the simulated results of the steering-angle response for a desired heading angle of 20° with $K_p = 1.0$ when the vehicle is moving at 1.7 m/s.

The cornering stiffness of the tyres is the most critical parameter of the developed model and can vary in real-time operation. Therefore, the variation in the estimated cornering stiffness of the tyres discussed in the section on determination of the vehicle parameters was also considered for sensitivity analysis. However, it was found from simulations using IPG: CarMaker that the experimental vehicle rolled over if the steering angle is greater than 7° at a longitudinal speed of 10 m/s. Hence, experiments could not be conducted at higher speeds because of safety constraints. This restricted the speeds at which experimental evaluations could be performed. For further analysis, simulations were carried out at a longitudinal speed of 10 m/s, and the results for the vehicle's heading angle are compared in Figure 17. The required steering angles are shown in Figure 18. It was found that, at 10 m/s, the proportional gain K_p has
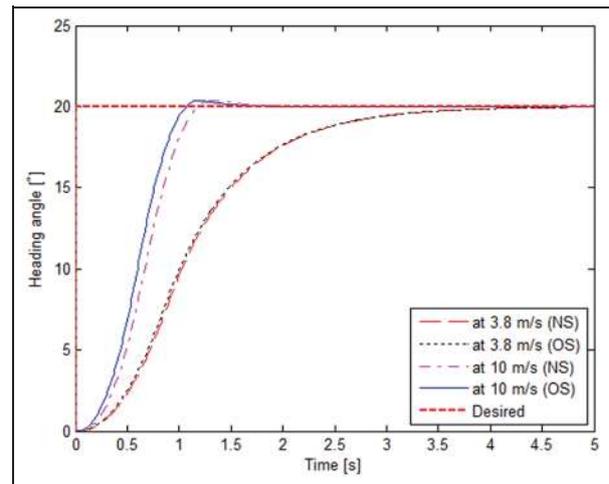

Figure 17. Comparison of the simulated results of the heading-angle response for a desired heading angle of 20° with a proportional controller ($K_p = 0.54$) when the vehicle is moving at 10 m/s.
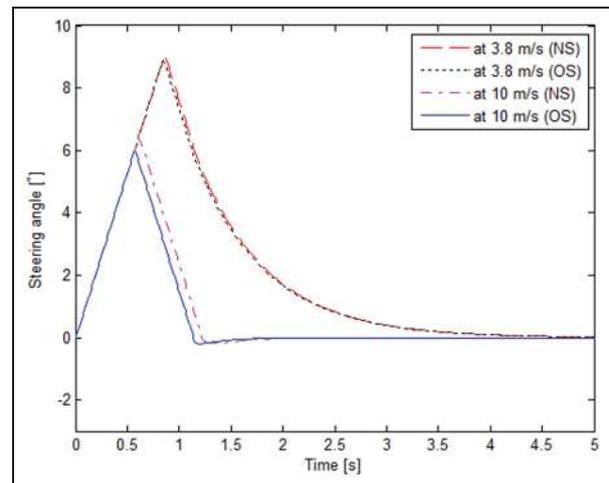NS: neutral steering; OS: oversteering.

Figure 18. Comparison of the simulated results of the steering-angle response for a desired heading angle of 20° with $K_p = 0.54$ when the vehicle is moving at 10 m/s.
NS: neutral steering; OS: oversteering.

to be reduced to 0.54 to meet the design criteria. The results for several test conditions are presented in Figures 17 and 18 to illustrate the performance of the developed controller. There was no difference between the performances for the neutral-steering model and the oversteering model of the AGV at low speeds. However, it was found that there was a significant difference between the performances for the neutral-steering model and the oversteering model of the vehicle at 10 m/s.

Optimal linear quadratic regulator for the desired heading angle

In order to compare the performance of the transfer-function-based proportional controller, a heading-angle
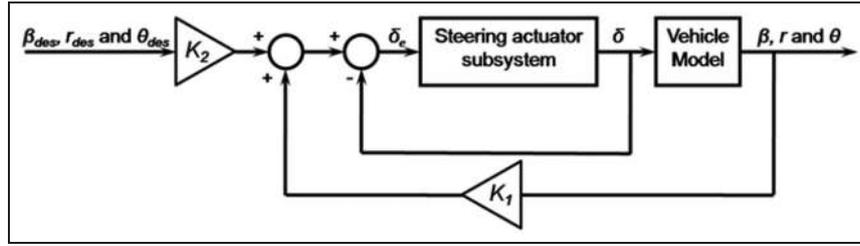
Figure 19. Optimal LQR framework.

controller using the optimal LQR framework as shown in Figure 19 was developed and evaluated. However, the experimental implementation of the LQR method requires a special optical sensor[14] to measure the side-slip angle of the vehicle. Because of the unavailability of this special optical sensor, the LQR controller was implemented on a simulation platform equipped with IPG: CarMaker simulation software for evaluation. Considering the cornering stiffness of the tyres to be normalized by the vertical load, the vehicle motion in equation (17) can be represented in state-space form as

$$\begin{bmatrix} \dot{\beta} \\ \dot{r} \\ \dot{\theta} \end{bmatrix} = \begin{bmatrix} -\frac{C_f + C_r}{m v_x} & -1 & 0 \\ 0 & -\frac{C_f l_f^2 + C_r l_r^2}{I_z v_x} & 0 \\ 0 & 1 & 0 \end{bmatrix} \begin{bmatrix} \beta \\ r \\ \theta \end{bmatrix} + \begin{bmatrix} \frac{C_f}{m v_x} \\ \frac{C_f l_f}{I_z} \\ 0 \end{bmatrix} \delta$$

(26)

Equation (26) can be represented as

$$\dot{q}(t) = \mathbf{A}q(t) + \mathbf{b}u(t)$$

and

$$y_1(t) = \mathbf{C}q(t)$$

(27)

where $q(t)$, $u(t)$ and $y_1(t)$ are the state vector, the control input and the measured output respectively. The state vector includes the side-slip angle, the yaw rate and the heading angle. The input is the steering angle. When a full-state feedback system is considered, the output includes the side-slip angle, the yaw rate and the heading angle. The aim of the LQR approach is to track and follow the desired heading angle as closely as possible while maintaining the steady-state yaw rate and the side-slip angle close to zero. The control error $\varepsilon(t)$, the desired parameters $z_1(t)$ and the performance output $y_1(t)$ are related by

$$\varepsilon(t) = z_1(t) - y_1(t)$$

(28)

For an infinite-horizon problem, the cost function J_c can be written as

$$J_c = \frac{1}{2} \int \left(\varepsilon^T \mathbf{Q}\varepsilon + Ru^2 \right) dt$$

(29)

where $\mathbf{Q}$ and R are the positive-definite weighting matrix on the tracking error and the positive-definite weighting scalar on the input error respectively. The optimal input consists of the sum of two components as given by

$$u^*(t) = \mathbf{k}_1 q(t) + \mathbf{k}_2 g(t)$$

(30)

In this equation, the first term is the full-state feedback with the Kalman gain $\mathbf{k}_1(t) = R^{-1}\mathbf{b}^T\mathbf{P}(t)$, where $\mathbf{P}(t)$ satisfies the algebraic Riccati equation

$$\mathbf{A}\mathbf{P} + \mathbf{P}\mathbf{A}^T - \mathbf{P}\mathbf{b}R^{-1}\mathbf{b}^T\mathbf{P} + \mathbf{C}^T\mathbf{Q}\mathbf{C} = 0$$

(31)

for an infinite-horizon linear quadratic problem, and the second term uses the auxiliary function $g(t)$ which is found from the solution of the differential equation

$$\dot{g}(t) = \left(\mathbf{A}^T - \mathbf{P}\mathbf{b}R^{-1}\mathbf{b}^T \right) g(t) + \mathbf{C}^T\mathbf{Q}z_1(t)$$

(32)

As $\dot{g}(t) = 0$, $g(t)$ can be written as

$$g(t) = -\left(\mathbf{A}^T - \mathbf{P}\mathbf{b}R^{-1}\mathbf{b}^T \right)^{-1}\mathbf{C}^T\mathbf{Q}z_1(t)$$

Therefore, $\mathbf{k}_2$ can be written as

$$\mathbf{k}_2 = -R^{-1}\mathbf{b}^T\left(\mathbf{A}^T - \mathbf{P}\mathbf{b}R^{-1}\mathbf{b}^T \right)^{-1}\mathbf{C}^T\mathbf{Q}$$

(33)

In this study, for a longitudinal velocity of the vehicle of 3.8 m/s, $\mathbf{k}_1$ and $\mathbf{k}_2$ were found to be

$$\begin{aligned} \mathbf{k}_1 &= \begin{bmatrix} 0.1427 & 1.0075 & 2.4495 \end{bmatrix} \\ \mathbf{k}_2 &= \begin{bmatrix} 0 & 0 & 2.4495 \end{bmatrix} \end{aligned}$$

(34)

The corresponding results from the experimental implementation and simulations are compared in Table 7. In this table, the 'proportional' controller refers to the controller developed using the classical transfer-function-based method. The settling time to reach the desired heading angle, the steady-state error and the maximum steering angle required are presented in Table 7. The heading-angle responses of the vehicle for various methods when the vehicle is moving at 3.8 m/s are shown in Figure 20. The corresponding steering-angle (control input) requirements are shown in Figure 21.

It was observed from Table 7 that the settling time can be reduced from 2.7 s to 2.3 s using an LQR controller. The proportional controller designed using the classical transfer-function-based method required only the heading angle as feedback. Additionally, it can be observed from Table 7 that the LQR method provides a slightly improved performance (in terms of the

Table 7. Evaluation of the LQR and proportional controllers for different test platforms to achieve a desired heading angle of 20°
when the vehicle is moving at 3.8 m/s.

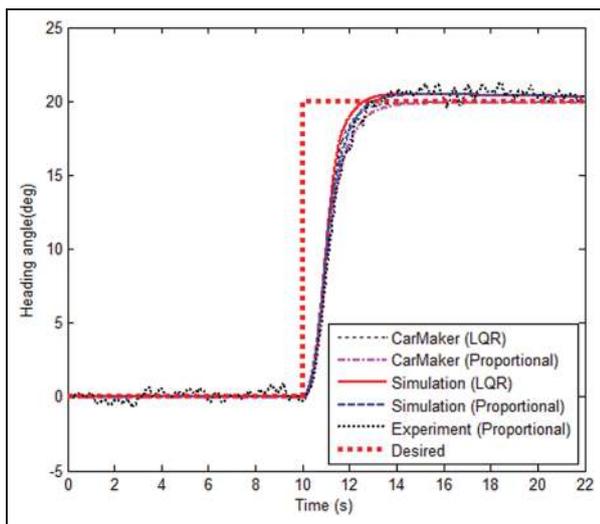| Test platform (controller)	Settling time (s)	Steady-state error (%)	Maximum steering angle required (deg)
CarMaker (LQR)	2.3	0.23	10.1
CarMaker (proportional)	2.7	0.73	9.3
Simulations (LQR)	2.0	0.1	9.9
Simulations (proportional)	2.3	0.1	9.2
Experiment (proportional)	2.7	2.70	10.2

LQR: linear quadratic regulator.

Figure 20. Comparison of the heading-angle responses of the vehicle for various methods when the vehicle is moving at 3.8 m/s.
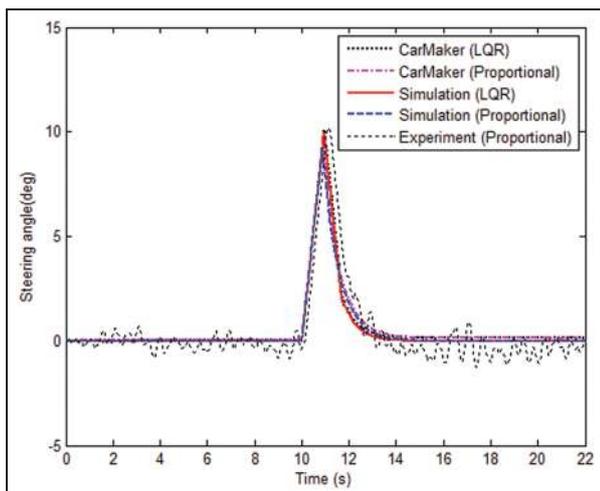LQR: linear quadratic regulator.

Figure 22. Heading-angle response using the LQR controller when the vehicle (CarMaker simulations) is moving at 10 m/s for different terrain adhesion coefficients to achieve a desired heading angle of 20°.

Figure 21. Comparison of the steering-angle responses of the vehicle for various methods when the vehicle is moving at 3.8 m/s.
LQR: linear quadratic regulator.

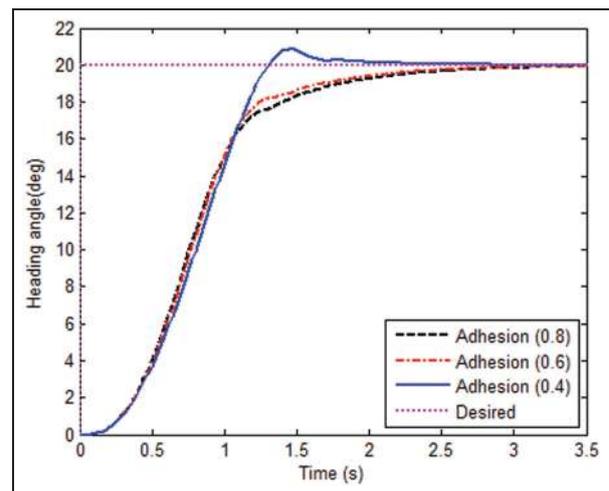settling time and the steady-state error), but the requirement of side-slip angle measurement is a constraint in its real-time implementation. In the absence of such a sensor, it can be observed that the classical transfer-function-based method is well suited to practical implementation since it provides a comparable performance without a significant increase in the maximum steering angle (which is the control input).

Influence of the adhesion coefficient at higher speeds

To evaluate the influence of the adhesion coefficient, the LQR controller was considered. While tracking the desired heading angle of the vehicle, the LQR controller ensures that the side-slip angle and the yaw rate of the vehicle remain close to zero as the time increases. The simulated results from the IPG: CarMaker simulation software when the vehicle is moving at 3.8 m/s and 10 m/s on terrains with different adhesion coefficients are shown in Table 8.

As shown in Table 8, when the longitudinal speed increased from 3.8 m/s to 10 m/s, the maximum steering requirement decreased from 10.13° to 6.27° to achieve a desired heading angle of 20°. The maximum side-slip angles of the tyres were found to vary from 0.7° to 2.7°.

Table 8. Evaluation of the LQR controller on the IPG: CarMaker simulation software for different terrain adhesion coefficients to achieve a desired heading angle of 20° when the vehicle is moving at 3.8 m/s and 10 m/s.

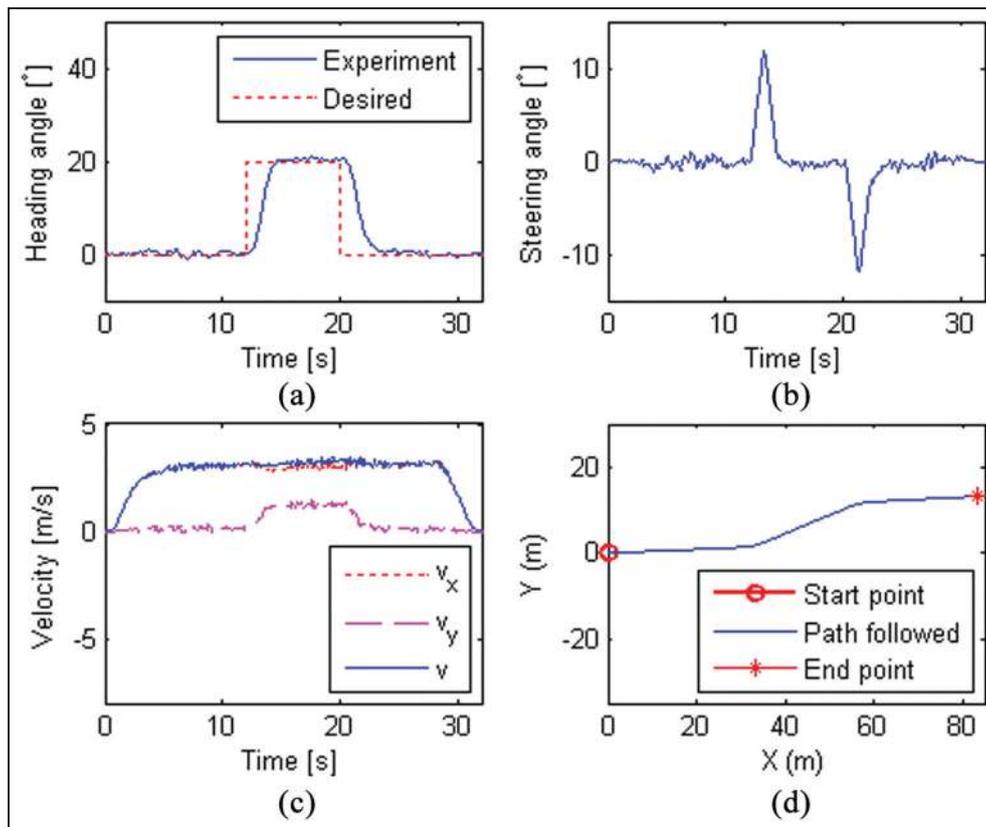| Vehicle speed (m/s)	Terrain adhesion coefficient	Settling time (s)	Steady-state error (%)	Maximum steering angle required (deg)
3.8	0.8	2.29	0.23	10.13
	0.6	2.28	0.23	10.15
	0.4	2.25	0.23	10.18
	0.2	2.12	0.24	10.40
10	0.8	1.80	0.10	6.27
	0.6	1.68	0.10	6.36
	0.4	1.22	0.10	6.80

Figure 23. (a) Heading-angle responses, (b) steering-angle responses, (c) velocity responses and (d) bird's eye view of the vehicle trajectory for a lane-change manoeuvre.

Thus, a linear model for the lateral force of the tyres can be used since the side-slip angle was less than 5°.

It was found that, at a speed of 3.8 m/s, a single gain matrix can be used for different terrain adhesion coefficients from 0.2 to 0.8. Similarly, at 10 m/s, a single gain matrix can be used for adhesion coefficients from 0.4 to 0.8. However, the gain matrix had to be retuned for the terrain adhesion coefficient of 0.2 at this speed. The corresponding heading-angle response from the IPG: CarMaker simulation software using the LQR controller is shown in Figure 22. These results indicate that the heading angle of the AGV can be controlled on different terrains using the LQR controller, but the experimental implementation can be carried out only when a

side-slip angle sensor is available on the experimental vehicle.

Lane-change manoeuvre

To check further the efficacy of the designed controller, a lane-change manoeuvre was carried out. Figure 23 shows the responses of the heading angle, the controlled steering angle, the velocities in the longitudinal and lateral directions and the bird's eye view of the vehicle trajectory for this lane-change manoeuvre. Initially, the vehicle was driven in a straight line for 12 s to achieve a speed of 3.1 m/s. Then, changes of 20° in the heading angle were made at the 12th second and the 20th second

to complete the task. A proportional controller gain $K_p = 0.8$ (see Table 6) was used for the lane-change manoeuvre. As discussed in the previous section, the AGV needs a time of nearly 3 s to achieve the desired heading angle. Therefore, when the vehicle is driven at 3.1 m/s, at least a 3 s gap is required to perform the next command; otherwise, the error in the desired heading angle is accumulated for consecutive waypoints and the vehicle deviates from its planned path. For autonomous navigation, knowledge of the heading-angle response which depends on the longitudinal velocity of the vehicle would be helpful in selection of the waypoints for discretization of the AGV route.

Conclusions

In this paper, a control-oriented model was used to design controllers to track the heading angle of an AGV for different terrain adhesion coefficients at various speeds. This was used to develop a classical transfer-function-based proportional controller and an LQR controller for tracking the desired heading angles. The proposed method was evaluated on a test vehicle using the following:

(a) an open-loop J-turn manoeuvre for corroborating the system model;
(b) tracking of the desired heading angle;
(c) a lane-change manoeuvre.

The developed controllers (a classical transfer-function-based proportional controller and an LQR controller) were evaluated using the IPG: CarMaker simulation platform over a range of speeds, and the proportional controller was also implemented on the experimental test vehicle at low speeds. The following conclusions were drawn from this study.

1. For low-speed navigation of an AGV, the heading-angle controller response was more sensitive to the speed of the vehicle than to the cornering stiffness of the tyres.
2. It was observed that the controller gain is reduced as the speed increases. Therefore, the controller gain needs to be retuned for different speeds, and a gain-scheduling method was considered.
3. When the vehicle is moving at a longitudinal speed between 1.7 m/s and 3.8 m/s, a change of 20° in the heading angle can be achieved on the experimental vehicle within 3.2 s with 5% steady-state error.
4. It was found that a single gain matrix could be used with the LQR-based controller for different terrain adhesion coefficients from 0.4 to 0.8.

Acknowledgements

Declaration of conflict of interest

Funding

References

1. Diaz-Calderon A and Kelly A. On-line stability margin and attitude estimation for dynamic articulating mobile robots. *Int J Robotics Res* 2005; 24(10): 845–866.
2. Hellström T and Ringdahl O. Follow the past: a path-tracking algorithm for autonomous vehicles. *Int J Veh Autonomous Systems* 2006; 4: 216–224.
3. Howard TM, Green CJ, Kelly A et al. State space sampling of feasible motions for high-performance mobile robot navigation in complex environments. *J Field Robotics* 2008; 25: 325–345.
4. Urmson C, Anhalt J, Bagnell D et al. Autonomous driving in urban environments: Boss and the urban challenge. *J Field Robotics* 2008; 25(8): 425–466.
5. Ferguson D, Howard TM and Likhachev M. Motion planning in urban environments: Part I. In: *IEEE/RSJ international conference on intelligent robots and systems*, Nice, France, 22–26 September 2008, pp. 1063–1069. New York: IEEE.
6. Bakker E, Nyborg L and Pacejka HB. Tyre modelling for use in vehicle dynamics studies. SAE paper 870421, 1987.
7. Dubins LE. On curves of minimal length with a constraint on average curvature and with prescribed initial and terminal positions and tangents. *Am J Math* 1957; 79: 497–516.
8. Reeds JA and Shepp RA. Optimal paths for car that goes both forward and backward. *Pacif J Math* 1990; 145(2): 367–393.
9. Schroder J, Gindele T, Jagszent D and Dillmann R. Path planning for cognitive vehicles using risk maps. In: *IEEE intelligent vehicles symposium*, Eindhoven, The Netherlands, 4–6 June 2008, pp. 1119–1124. New York: IEEE.
10. Coombs D, Murphy K, Lacaze A and Legowik S. Driving autonomously off-road up to 35 km/h. In: *IEEE intelligent vehicles symposium*, Dearborn, Michigan, USA, 3–5 October 2000, pp. 186–191. New York: IEEE.
11. Suppachai H, Silawatchananai C, Parnichkun M and Wuthishuwong C. Double loop controller design for the vehicle's heading control. In: *IEEE international conference on robotics and biomimetics*, Guilin, People's Republic of China, 19–23 December 2009, pp. 989–994. New York: IEEE.
12. Lee MH, Lee KS, Park HG et al. Robust lateral controller for an unmanned vehicle via a system identification

method. *J Mech Systems Transpn Logistics* 2010; 3(3): 504–520.

13. Kim J, Lee H and Choi S. A robust road bank angle estimation based on a proportional–integral H_∞ filter. *Proc IMechE Part D: J Automobile Engineering* 2012; 226(6): 779–794.

14. Wesemeier D and Isermann R. Identification of vehicle parameters using stationary driving maneuvers. *Control Engng Practice* 2009; 17: 1426–1431.

15. Sierra C, Tseng E, Jain A et al. Cornering stiffness estimation based on vehicle lateral dynamics. *Veh System Dynamics* 2006; 44: 24–38.

16. Rezai M and Shirazi KH. Robust handling enhancement on a slippery road using quantitative feedback theory. *Proc IMechE Part D: J Automobile Engineering* 2014; 228(4): 426–442.

17. Kutluay E and Winner H. Validation of vehicle dynamics simulation models – a review. *Veh System Dynamics* 2014; 52: 186–200.

18. Kazemi M and Shirazi KH. Handling enhancement of a sliding-mode control assisted four-wheel steer vehicle. *Proc IMechE Part D: J Automobile Engineering* 2012; 226(2): 234–246.

19. Ba T, Guan X and Zhang J. Vehicle predictive control based on the recursive subspace identification method. *Proc IMechE Part D: J Automobile Engineering* 2015; 229(8): 1094–1109.

20. Du H, Zhang N and Naghdy F. Velocity-dependent robust control for improving vehicle lateral dynamics. *Transpn Res Part C* 2011; 19: 454–468.

21. Mirzaei M. A new strategy for minimum usage of external yaw moment in vehicle dynamic control system. *Transpn Res Part C* 2010; 18: 213–224.

22. Attia R, Orjuela R and Basset M. Combined longitudinal and lateral control for automated vehicle guidance. *Veh System Dynamics* 2014; 52: 261–279.

23. Janbakhsh AA, Khaknejad MB and Kazemi R. Simultaneous vehicle-handling and path-tracking improvement using adaptive dynamic surface control via a steer-by-wire system. *Proc IMechE Part D: J Automobile Engineering* 2013; 227(3): 345–360.

24. Yakub F and Mori Y. Comparative study of autonomous path-following vehicle control via model predictive control and linear quadratic control. *Proc IMechE Part D: J Automobile Engineering* 2015: in press.

25. NovaTel Inc. SPAN technology for OEMV user manual rev 11, Publication number OM-20000104, http://www.novatel.com/assets/Documents/Manuals/om-20000104.pdf (September 2012, accessed 27 May 2015).

26. Hewson P. Method of estimating tyre cornering stiffness from basic tyre information. *Proc IMechE Part D: J Automobile Engineering* 2005; 219(12): 1407–1412.

27. Gillespie TD. *Fundamentals of vehicle dynamics*. Warrendale, Pennsylvania: SAE International, 1992, pp. 347–355.

28. Sahoo S, Subramanian SC, Mahale N et al. Design and development of a heading angle controller for an unmanned ground vehicle. *Int J Automot Technol* 2015; 16(1): 27–37.

Appendix 1

Notation

a	tyre aspect ratio
b	thickness of the tyre belt
C_f	cornering stiffness of the front wheel
C_r	cornering stiffness of the rear wheel
E	compression modulus of the belt
F_{yf}	lateral tyre force on the front wheel
F_{yr}	lateral tyre force on the rear wheel
I_z	yaw moment of inertia of the vehicle
m	mass of the vehicle
l	wheelbase
l_f	distance of the front tyre from the centre of gravity of the vehicle
l_r	distance of the rear tyre from the centre of gravity of the vehicle
r	yaw rate of the vehicle
r_w	radius of the wheel
s	unitized percentage of the sidewall vertical deflection when loaded
v_x	longitudinal velocity of the vehicle
v_y	lateral velocity of the vehicle
w	width of the belt
α_f	slip angle of the front wheel
α_r	slip angle of the rear wheel
β	side-slip angle of the vehicle
δ	steering angle of the front wheel
θ	yaw angle of the vehicle measured with respect to the inertial global x axis
ϕ	angle of rotation of the steering motor shaft